Desalination and Water Treatment
www.deswater.com

doi: 10.5004/dwt.2018.21975

108 (2018) 369–375
March

Role of calcination in sol-gel synthesis of 5%In-0.05%Sm-TiO_2 for photocatalytic degradation of methyl orange

Wenjie Zhang*, Yingjie Tao, Xiaobei Pei

School of Environmental and Chemical Engineering, Shenyang Ligong University, Shenyang 110159, China,
Tel. +86 13609880790; emails: wjzhang@aliyun.com (W. Zhang), 2995910063@qq.com (Y. Tao), 976325658@qq.com (X. Pei)

Received 15 June 2017; Accepted 5 February 2018

ABSTRACT

Sol-gel method was used to prepare a novel 5%In-0.05%Sm-TiO_2 photocatalyst. The materials were characterized by XRD, SEM, FT-IR/FIR, UV–Vis diffuse reflectance, and N_2 adsorption–desorption analyses. Anatase phase TiO_2 is formed in all the samples while calcination temperature ranges from 350°C to 600°C. Cell volume of anatase TiO_2 slightly expands with rising calcination temperature. The band gap energies of the 5%In-0.05%Sm-TiO_2 samples calcined at 350°C, 400°C, 450°C, 500°C and 600°C are 2.84, 2.90, 2.91, 2.95 and 3.02 eV, respectively. Specific surface area of the samples gradually decreases with rising calcination temperature, while the average pore size and total pore volume constantly increase at the same time. The maximum photocatalytic activity is found on the sample calcined at 400°C. 97.7% of the initial methyl orange is removed from the solution after 45 min of irradiation. The conjugated chromophores in methyl orange molecule are almost decomposed at this time.

Keywords: TiO_2; Indium; Samarium; Photocatalysis; Methyl orange

1. Introduction

Photocatalytic oxidation of organic pollutants in wastewater has been studied for nearly half a century [1–3]. This technique has been applied to produce many kinds of environmentally functional materials. The application of photocatalytic oxidation in large-scale wastewater treatment plant is interesting. As for the two major factors influencing wastewater treating efficiency, that is, illumination and photocatalyst, materials with high photocatalytic activity are always the research focus. Despite the various types of materials, TiO_2 is the most studied one that has the greatest activity [4–6]. TiO_2-based materials can be utilized in almost all the fields relating to photocatalytic technique [7,8]. On the other hand, modification of TiO_2-based materials is capable of greatly improving their activity [9,10]. Metal ion doping into TiO_2 crystalline skeleton is a widely applied method [11–14]. Recombination of photogenerated electron–hole pairs can be retarded by the doped metal ions [15,16]. Photocatalytic activity of the TiO_2-based materials can be enhanced due to extending lifetime of the charge carriers.

Many elements have been used to modify TiO_2-based materials as dopants. Moreover, a recent attempt is to simultaneously dope two dopants into TiO_2 [17,18]. The combination and synergistic effect of two different elements are absolutely important. Tobaldi et al. [19] reported photocatalytic properties of TiO_2 nano-heterostructure after Cu-Zn modification. Kotesh et al. [20] studied Ag-Cu/TiO_2 photocatalyst under solar and artificial light for H_2O splitting. Sasani et al. [21] studied Mg-Nb co-doped TiO_2 with a preferred (101) anatase surface [21]. However, it is hard to say that co-doping of different elements is positive to improve activity of TiO_2-based materials.

The selection of two different types of elements is complex and the effects must be ascertained by experimental results. Rare earth metals are effective dopants in many photocatalytic materials. The combination of rare earth metal ions and main group element ions in TiO_2 is a new approach. The synthesis of a novel In-Sm co-doped TiO_2 material through sol-gel route was studied in this work. XRD, SEM, FT-IR/FIR,

* Corresponding author.

UV–Vis diffuse reflectance and N_2 adsorption–desorption analyses were conducted to the synthesized materials. The effects of calcination temperature on characterizations and photocatalytic activity of 5%In-0.05%Sm-TiO_2 materials were studied.

2. Experimental methods

2.1. Synthesis of 5%In-0.05%Sm-TiO_2

In-Sm co-doped TiO_2 was synthesized through a sol-gel route. 0.9 mL distilled water and 4 mL anhydrous ethanol were mixed to form a transparent solution. 8 mL anhydrous ethanol and 0.1 mL concentrated hydrochloric acid were mixed in another beaker, followed by addition of 2 mL tetrabutyl titanate, $Sm(NO_3)_3$ and $In(NO_3)_3$. After the second solution became transparent under stirring, it was mixed with the first solution. A transparent sol formed after 30 min, and then a sticky gel formed after stirring for about 1 h. After staying at ambient temperature for 12 h, the gel was dried at 80°C in the furnace for another 12 h. The obtained solid was transferred into an oven. The oven was heated at 5°C/min to the desired calcination temperature. The powders were calcined for 3 h.

2.2. Characterization of photocatalysts

Crystal structure of materials was analyzed by D8 Advance X-ray diffractometer at 40 kV and 40 mA for monochromatized Cu Kα (λ = 1.5416 Å) radiation. The surface morphology was observed by QUANTA 250 scanning electron microscope at an accelerating voltage of 30 kV. A thin layer of gold was coated on the samples to avoid charging. Infrared and far infrared absorption spectra were recorded by a Frontier FT-IR/FIR spectrometer in the wavenumber between 50 and 4,000 cm^{-1}. UV–Vis diffuse reflectance spectra were recorded by LAMBDA 35 UV–Vis spectrometer equipped with an integrating sphere. The spectra were measured using $BaSO_4$ as a reference and were transformed from reflection to absorbance by the Kubelka-Munk method. Specific surface area and pore characters of the materials were measured by an F-sorb 3400 analyzer through N_2 adsorption–desorption.

2.3. Decoloration of methyl orange

Decoloration of methyl orange (MO) was measured to study the activity of 5%In-0.05%Sm-TiO_2. A 100 mL quartz beaker and a 20 W UV-light lamp irradiating at 253.7 nm were set up as the lab-scale reactor. 15 mg photocatalyst and 50 mL of 10 mg/L MO solution were used in each experiment. Prior to turning on the light, the suspension was ensured adsorption–desorption equilibrium after stirring in the dark for 60 min. Adsorption percent of MO on the photocatalyst was measured at this moment. The average irradiation intensity was 1,300 $\mu W/cm^2$, as measured on the surface of the suspension using an actinometer. The irradiation time in the subsequent experiments was set to 30 min except for the prolonged time reaction. Absorbance of the solution was measured by a 721E spectrophotometer at the maximum absorption wavelength of MO, that is, 466 nm. Photocatalyst was removed from the solution through a Millipore filter. MO concentration was calculated according to Lambert–Beer theory.

3. Results and discussion

3.1. Characterization results

Fig. 1 shows XRD patterns of 5%In-0.05%Sm-TiO_2 samples that were prepared at different calcination temperatures. All the diffraction patterns belong to anatase phase TiO_2 despite the difference in calcination temperature ranging from 350°C to 600°C. The diffraction peaks of rutile phase TiO_2 are not found in the patterns. Phase transformation from anatase to rutile does not happen at the given temperature. Crystallite formation of anatase TiO_2 is favored at relatively high temperature, as indicated by the sharpening of the diffraction peaks with rising calcination temperature. Crystallite size of the TiO_2 (101) plane is calculated from Scherrer formula. The crystallite sizes of the 5%In-0.05%Sm-TiO_2 samples are 8.7, 8.9, 10.2, 11.3 and 13.4 nm when the calcination temperatures are at 350°C, 400°C, 450°C, 500°C and 600°C, respectively. High temperature treatment is beneficial to formation and growing of TiO_2 crystals.

Lattice parameters of 5%In-0.05%Sm-TiO_2 samples are calculated from the diffraction patterns, as listed in Table 1. Cell volume of anatase TiO_2 slightly expands with

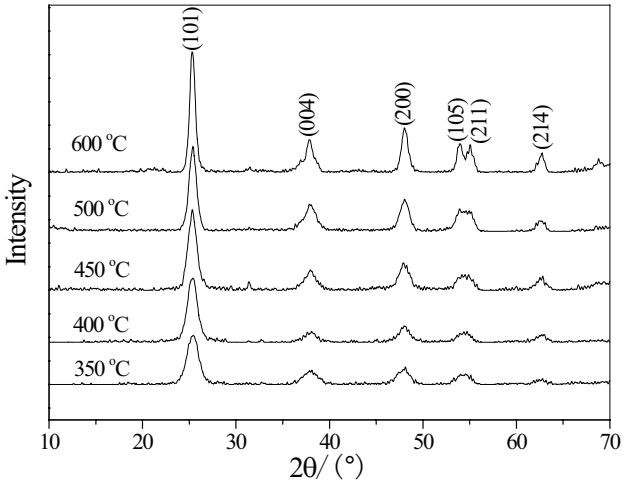

Fig. 1. XRD patterns of 5%In-0.05%Sm-TiO_2 samples calcined at different calcination temperatures.

Table 1
Lattice parameters of 5%In-0.05%Sm-TiO_2 samples as a factor of calcination temperature

Temperature (°C)	a(=b) (10^{-1} nm)	c (10^{-1} nm)	V (10^{-3} nm^3)
350	3.7209	9.4266	130.52
400	3.7624	9.3839	133.68
450	3.7781	9.3742	133.81
500	3.7849	9.3619	134.12
600	3.7887	9.3541	134.27

rising calcination temperature, indicating crystal growth during thermal treatment. Meanwhile, lattice parameters *a* and *b* are enlarged at higher temperature, while lattice parameter *c* encounters a reverse trend. That means the cell expands at two dimensions and shrinks at the third dimension. This might cause the reduction of lattice distance in the third dimension, which can also be indicated by the shifting of diffraction peaks to the larger angle. Substances containing indium and samarium cannot be distinguished in the XRD patterns, although the indium doping content is as high as 5% in the 5%In-0.05%Sm-TiO_2. Similar result is reported in our previous work using aluminum and indium as dopants [22].

Surface morphologies of 5%In-0.05%Sm-TiO_2 samples are shown in Fig. 2. The particles in all the samples are irregular in shape and with different particle size. The TiO_2 crystals tend to aggregate together to form large particles during sol-gel synthesizing process. The particle size becomes larger after being calcined at higher thermal temperature. Meanwhile, there are also smaller particles scattering among the large ones, partly as the result of grinding after calcination.

FT-IR and FT/Far IR spectra of 5%In-0.05%Sm-TiO_2 samples are shown in Fig. 3. The adsorbed hydroxyl groups can be distinguished by the stretching and bending vibrations of O–H bond at 3,422 and 1,641 cm^{-1} [23,24]. Surface adsorbed hydroxyl is important to photocatalytic generation of holes after electron exciting. Although the materials are dried before IR examination to remove the adsorbed water molecules, there is still detectable hydroxyl group combining with TiO_2. The absorption of stretching vibration of C–O bond is also found at 1,387 cm^{-1} [25]. The absorption intensity of O–H bond becomes a little weaker after calcining at higher temperature. At the same time, the removal of organic substances

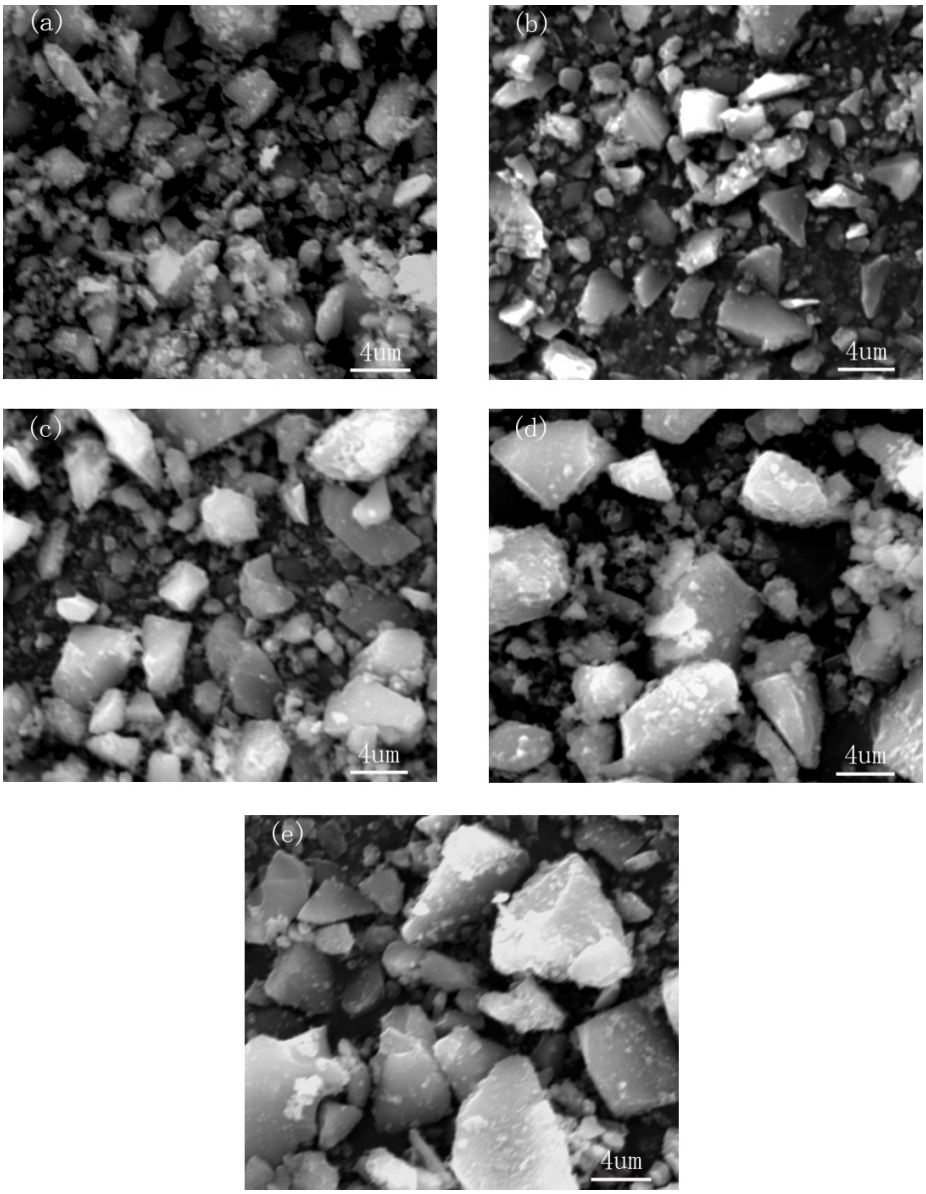

Fig. 2. SEM images of 5%In-0.05%Sm-TiO_2 samples calcined at different temperatures. (a) 350°C, (b) 400°C, (c) 450°C, (d) 500°C and (e) 600°C.

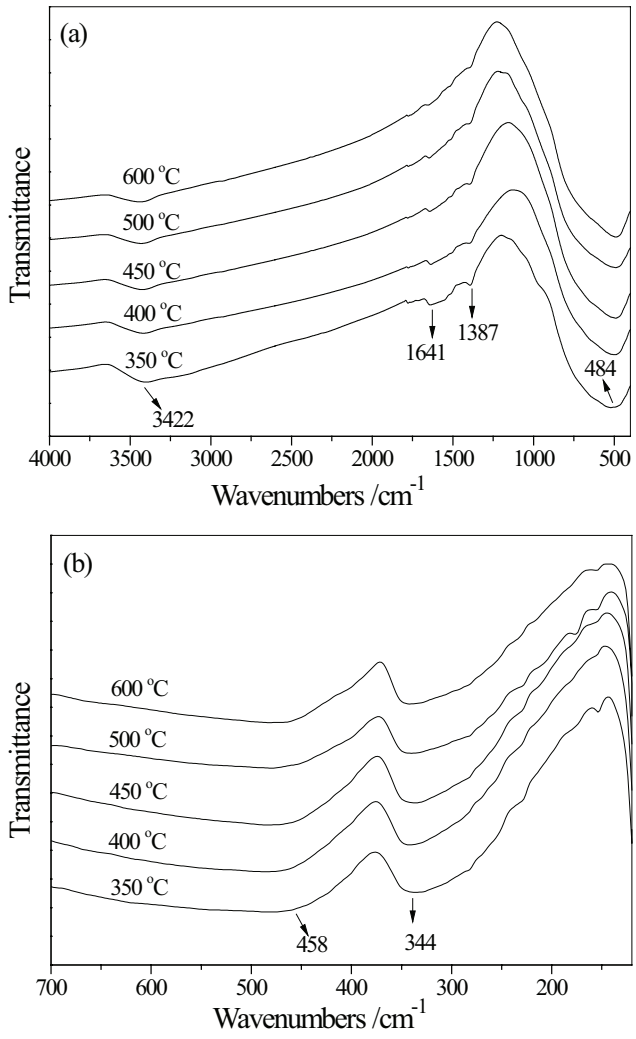

Fig. 3. (a) FT-IR and (b) Far IR spectra of 5%In-0.05%Sm-TiO_2 samples with respect to calcination temperature.

can also be proven by the shrinking absorption intensity of C–O bond.

FT-far IR spectra are used to ascertain metal–oxygen bondings in the 5%In-0.05%Sm-TiO_2 samples. The broad absorptions centered at 458 and 344 cm^{-1} are attributed to bending vibration of Ti-O-Ti [26]. The variation of calcination temperature does not noticeably influence the bonding characters of TiO_2. The major skeleton of anatase TiO_2 lattice forms at relatively low temperature and does not change with rising calcination temperature.

UV–Vis diffuse reflectance spectra of 5%In-0.05%Sm-TiO_2 are illustrated in Fig. 4. The band gap energies of the semiconductors can be calculated using Tauc plot method [27]. All samples have strong absorption in the ultraviolet region. The increase of calcination temperature leads to a continuous red shift of the absorption edges. The band gap energies of the 5%In-0.05%Sm-TiO_2 samples that were calcined at 350°C, 400°C, 450°C, 500°C and 600°C are 2.84, 2.90, 2.91, 2.95 and 3.02 eV, respectively. The synthesized pure TiO_2 in this work has a band gap of 3.08 eV. The doping of indium and samarium leads to a slight red shift of the band gap energy.

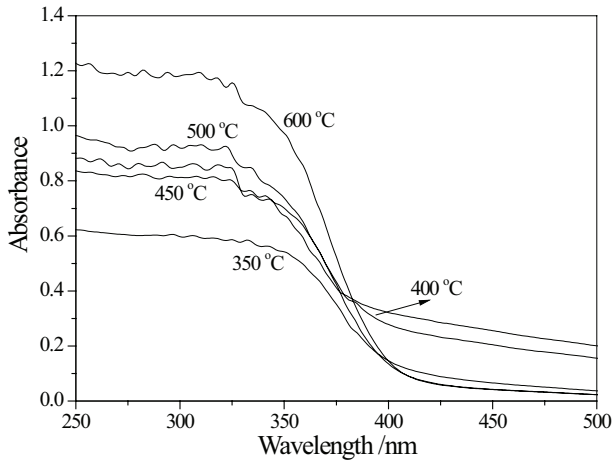

Fig. 4. UV–Vis diffuse reflectance spectra of 5%In-0.05%Sm-TiO_2 samples.

On the other hand, all the samples contain equal amount of dopants in the TiO_2 base materials. The variation of band gap energy with rising calcination temperature can be attributed to the change in crystallite size during thermal treatment. Crystallite size expansion of TiO_2 is usually accompanied with enlarging band gap energy. The slight variation of band gap energy is not believed to put much effect on photo-exciting of electrons in the valence band, since the lamp in this work can irradiate photon at the wavelength of 253.7 nm. The photons possess enough energy to excite all the samples in this work.

N_2 adsorption–desorption method is used to measure the specific area and porous structure of 5%In-0.05%Sm-TiO_2 samples. Desorption isotherms are presented in Fig. 5. As can be seen in the figure, the prepared sample at low temperature can adsorb more N_2 molecules. The desorption isotherms of the calcined samples at 350°C and 400°C represent a typical mesoporous structure. All the materials contain certain amount of macropores, which can be proved by the abrupt increasing adsorption at relative pressure near 1.0.

Table 2 gives specific surface area and porous characters of 5%In-0.05%Sm-TiO_2 at different temperatures. Specific surface area of the samples gradually decreases with rising calcination temperature, whereas the average pore size and total pore volume constantly increase at the same time. Organic substances in the gel are removed through oxidation during thermal treatment, leaving porous structure in the produced solid powders. Small mesopores are formed at relatively low temperature. There are still some organic residues remaining in the materials, resulting the large surface area and small pore size. When calcination temperature increases, crystal formation and growing are accompanied with crystal aggregation. The small pores merge into large pores in this stage. Crystal growing and pore expansion are the two major factors that lead to shrinking surface area at high temperature.

3.2. Photocatalytic degradation of methyl orange on 5%In-0.05%Sm-TiO_2

Methyl orange was used as a probe substance to measure the photocatalytic activity of 5%In-0.05%Sm-TiO_2.

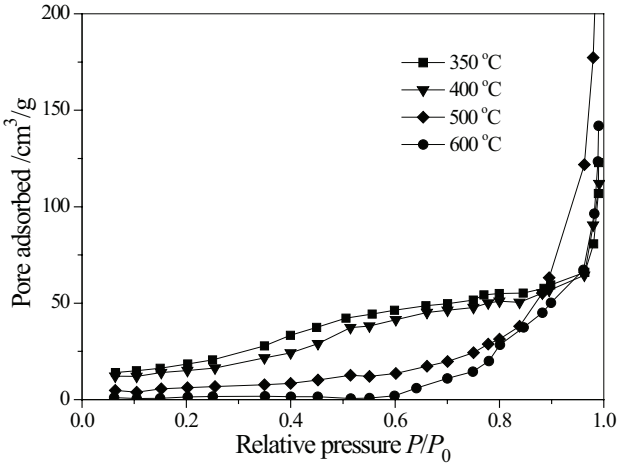

Fig. 5. N_2 desorption isotherms of 5%In-0.05%Sm-TiO_2.

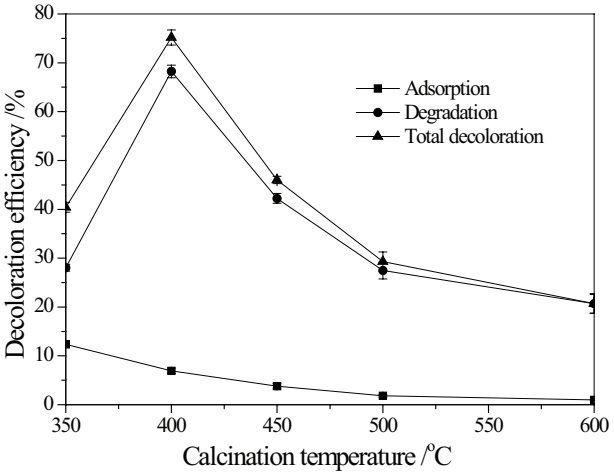

Fig. 6. Photocatalytic activities of 5%In-0.05%Sm-TiO_2 samples as a factor of calcination temperature.

Table 2
Specific surface area and porous characters of 5%In-0.05%Sm-TiO_2 calcined at different temperatures

Temperature (°C)	BET surface area (m^2/g)	Average pore size (nm)	Pore volume (cm^3/g)
350	136.5	10.8	0.2186
400	113.1	12.5	0.2312
450	63.6	20.5	0.2928
500	51.7	30.6	0.3218
600	21.4	45.3	0.4383

Fig. 6 shows adsorption and photocatalytic degradation of MO on 5%In-0.05%Sm-TiO_2 as a factor of calcination temperature. The sample calcined at 350°C can adsorb as much as 12.4% of the initial MO molecules on its surface after adsorption–desorption equilibrium. The adsorption percentage constantly declines when the calcination temperature increases from 350°C to 600°C. The adsorption capacity is in close relationship to the specific surface area of the materials. The adsorption of MO molecules can only contribute to a small part of removing the dye from the solution.

The sample calcined at 350°C has comparatively weak activity on photocatalytic degradation of MO. Although anatase TiO_2 crystal begins to form at this low temperature, crystallization of anatase TiO_2 is insufficient. The remaining organic residues in the material are detrimental to photon absorption. The maximum photocatalytic activity is found on the sample calcined at 400°C. The degradation efficiency is as high as 69.8% after 30 min of illumination. However, the samples calcined at higher temperatures encounter a sharp reducing activity on MO degradation.

Calcination is a key process in sol-gel synthesizing of TiO_2-based materials. Crystallization, phase transformation, particle aggregation and pore forming can be affected by the variation of calcination temperature. A material of well crystallization, fine crystallite size, porous structure and large surface area usually has strong photocatalytic activity on degradation of organic substances. As the result, there is always an optimal thermal treating temperature of synthesizing the material. The above mentioned complex effects must be considered in order to clarify the influence of calcination.

Fig. 7(a) shows the removal of MO with extending irradiation time on 5%In-0.05%Sm-TiO_2 that is calcined at 400°C. The solution containing photocatalyst powders and MO molecules were stirred in the dark for 60 min to ensure adsorption–desorption equilibrium. Photocatalytic degradation of MO is initiated after turning on the lamp. 97.7% of the initial MO is removed from the solution after 45 min of irradiation. Although the adsorption of the dye on the surface of the photocatalyst can also remove some MO molecules from the solution, photocatalytic degradation is the major dye decoloration way. Photogenerated electrons, holes and various subsequently produced oxidation species react with MO molecules for the subsequent degradation.

Fig. 7(b) shows the UV–Vis absorption spectra of MO solution during photocatalytic degradation on 5%In-0.05%Sm-TiO_2. The absorptions of MO molecule in visible and ultraviolet regions can be used to indicate the degradation process. A strong and broad absorption peak centering at 466 nm in the visible region is often used to measure the concentration of MO solution. This absorption is related to the conjugated chromophores group in MO molecule. There are several weak absorption peaks caused by MO in the ultraviolet region. These absorptions are due to the benzene ring in MO molecule. As a typical azo dye, MO is known as its orange juice-like color. After this dye is discharged into the aquatic system, the wastewater can be readily distinguished by its apparent color even at considerably low concentration. Methyl orange aqueous solution has high absorption intensity in the visible region at low concentration.

Methyl orange molecules can be degraded into small fragments during photocatalytic process. After 60 min of illumination on 5%In-0.05%Sm-TiO_2, the broad absorption peak in the visible region nearly disappears in the spectrum. That means the conjugated chromophores in MO molecule are almost decomposed at this time. As a result, the MO solution is consequently decolorized. However, the total mineralization of the intermediate organic residues might require much longer time. There are still weak absorptions in the ultraviolet region of the spectra.

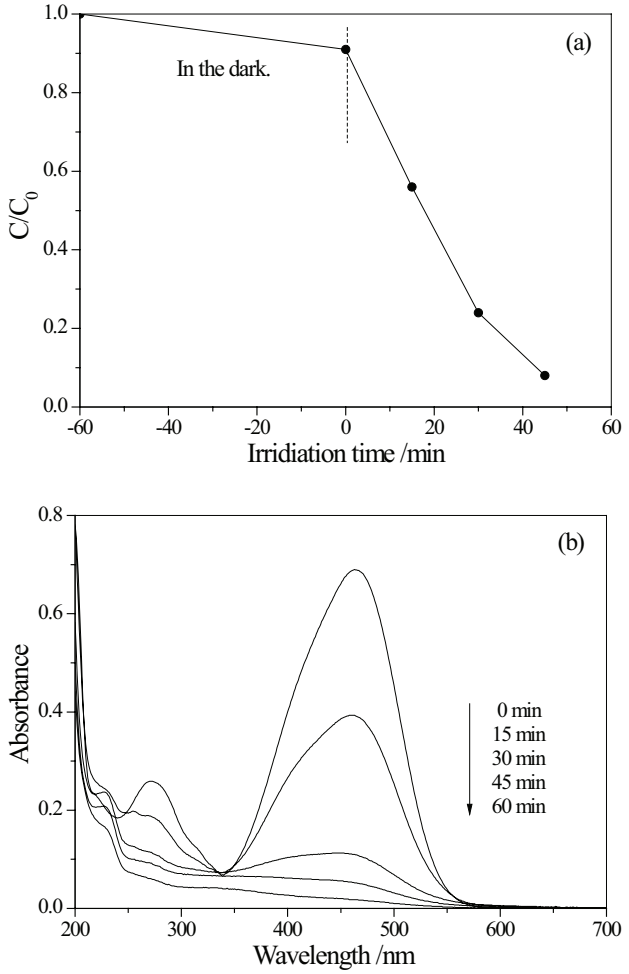

Fig. 7. (a) Degradation of methyl orange on 5%In-0.05%Sm-TiO_2 calcined at 400°C and (b) UV–Vis absorption spectra of MO aqueous solution catalyzed by 5%In-0.05%Sm-TiO_2.

Fig. 8 shows the effect of 5%In-0.05%Sm-TiO_2 dosage on the photocatalytic degradation efficiency. The initial MO solution is 10 mg/L. Degradation efficiency is enhanced after using more 5%In-0.05%Sm-TiO_2 photocatalyst when the dosage is low. The maximum degradation efficiency is obtained at 5%In-0.05%Sm-TiO_2 dosage of 200 mg/L. 67.4% of the dye can be degraded after 30 min of irradiation. Further increase of photocatalyst dosage encounters a slightly reducing efficiency. A similar phenomenon is often observed in the suspension containing photocatalyst powders. Fine photocatalyst powders tend to aggregate into large particles at high dosage.

4. Conclusions

In-Sm co-doped TiO_2 was synthesized through a sol-gel route. The effects of calcination temperature on characterizations and photocatalytic activity of 5%In-0.05%Sm-TiO_2 materials were studied. All the samples are composed of anatase phase TiO_2 despite the difference in calcination temperatures. Substances containing indium and samarium are not found in the XRD patterns. Cell volume of anatase TiO_2 slightly expands with rising calcination temperature. FT-far IR spectra ascertain Ti-O-Ti bonding in the 5%In-0.05%Sm-TiO_2 samples. The increase of calcination temperature leads to a continuous red shift of the UV–Vis absorption edges. Crystal growing and pore expansion are the two major factors that lead to shrinking surface area at high temperature. The sample calcined at 400°C has the maximum activity on MO photocatalytic degradation. The maximum degradation efficiency is obtained at 5%In-0.05%Sm-TiO_2 dosage of 200 mg/L.

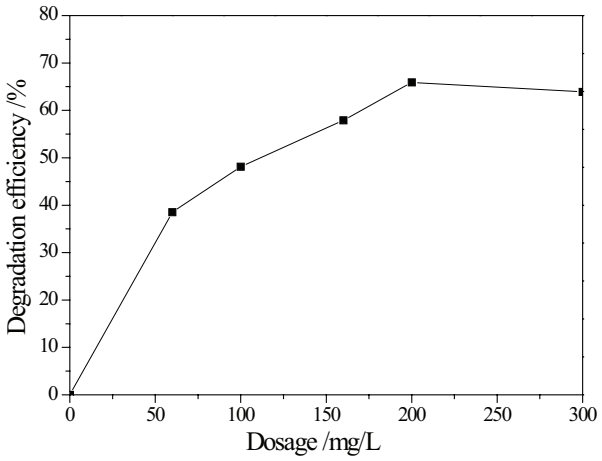

Fig. 8. Photocatalytic degradation of methyl orange with respect to 5%In-0.05%Sm-TiO_2 dosage. The sample was calcined at 400°C.

Acknowledgments

This work was supported by the Natural Science Foundation of Liaoning Province (No. 2015020186) and the National Natural Science Foundation of China (No. 41571237).

References

[1] A. Fujishima, T.N. Rao, D.A. Tryk, Titanium dioxide photocatalysis, J. Photochem. Photobiol., C, 1 (2000) 1–21.
[2] W. Zhang, Y. Li, F. Wang, Properties of TiO_2 thin films prepared by magnetron sputtering, J. Mater. Sci. Technol., 18 (2002) 101–107.
[3] D. Chatterjee, S. Dasgupta, Visible light induced photocatalytic degradation of organic pollutants, J. Photochem. Photobiol., C, 6 (2005) 186–205.
[4] W. Zhang, Z. Ma, K. Li, L. Yang, H. Li, H. He, Sol-gel synthesis of nano-sized TiO_2 supported on HZSM-5, Curr. Nanosci., 12 (2016) 514–519.
[5] P. Zhou, J. Wu, W. Yu, G. Zhao, G. Fang, S. Cao, Vectorial doping-promoting charge transfer in anatase TiO_2 {0 0 1} surface, Appl. Surf. Sci., 319 (2014) 167–172.
[6] Y. Ku, S. Shiu, H. Wu, Decomposition of dimethyl phthalate in aqueous solution by UV–LED/TiO_2 process under periodic illumination, J. Photochem. Photobiol., A, 332 (2017) 299–305.
[7] M. Bellardita, A. Paola, B. Megna, L. Palmisano, Absolute crystallinity and photocatalytic activity of brookite TiO_2 samples, Appl. Catal., B, 201 (2017) 150–158.
[8] M. Tahir, B. Tahir, N. Saidina Amin, H. Alias, Selective photocatalytic reduction of CO_2 by H_2O/H_2 to CH_4 and CH_3OH over Cu-promoted In_2O_3/TiO_2 nanocatalyst, Appl. Surf. Sci., 389 (2016) 46–55.

[9] J.B. Cai, X.Q. Wu, S.X. Li, F.Y. Zheng, Controllable location of Au nanoparticles as cocatalyst onto TiO_2@CeO_2 nanocomposite hollow spheres for enhancing photocatalytic activity, Appl. Catal. B, 201 (2017) 12–21.
[10] W.K. Jo, S. Kumar, M.A. Isaacs, A.F. Lee, S. Karthikeyan, Cobalt promoted TiO_2/GO for the photocatalytic degradation of oxytetracycline and Congo Red, Appl. Catal. B, 201 (2017) 159–168.
[11] J. Yu, J. Xiong, B. Cheng, S. Liu, Fabrication and characterization of Ag-TiO_2 multiphase nanocomposite thin films with enhanced photocatalytic activity, Appl. Catal. B, 60 (2005) 211–221.
[12] J. Du, X. Li, K. Li, X. Gu, W. Qi, K. Zhang, High hydrophilic Si-doped TiO_2 nanowires by chemical vapor deposition, J. Alloys Compd., 687 (2016) 893–897.
[13] A. Juma, I.O. Acik, A.T. Oluwabi, A. Mere, V. Mikli, M. Danilson, M. Krunks, Zirconium doped TiO_2 thin films deposited by chemical spray pyrolysis, Appl. Surf. Sci., 387 (2016) 539–545.
[14] W. Zhang, X. Pei, B. Yang, H. He, Effects of boron content and calcination temperature on properties of B-TiO_2 photocatalyst prepared by solvothermal method, J. Adv. Oxid. Technol., 17 (2014) 66–72.
[15] E.B. Simsek, Solvothermal synthesized boron doped TiO_2 catalysts: photocatalytic degradation of endocrine disrupting compounds and pharmaceuticals under visible light irradiation, Appl. Catal. B, 200 (2017) 309–322.
[16] C. Han, J. Andersen, V. Likodimos, P. Falaras, J. Linkugel, D.D. Dionysiou, The effect of solvent in the sol–gel synthesis of visible light-activated, sulfur-doped TiO_2 nanostructured porous films for water treatment, Catal. Today, 224 (2014) 132–139.
[17] L. Chen, C. Huang, C. Gao, A comparative study of the effects of In_2O_3 and SnO_2 modification on the photocatalytic activity and characteristics of TiO_2, Chem. Eng. J., 175 (2011) 49–55.
[18] J. Liu, R. Han, H. Wang, Y. Zhao, W. Lu, H. Wu, Degradation of PCP-Na with La–B co-doped TiO_2 series synthesized by the sol–gel hydrothermal method under visible and solar light irradiation, J. Mol. Catal. A, 344 (2011) 145–152.
[19] D.M. Tobaldi, C. Piccirillo, N. Rozman, R.C. Pullar, M.P. Seabra, A.S. Škapin, P.M.L. Castro, J.A. Labrincha, Effects of Cu, Zn and Cu-Zn addition on the microstructure and antibacterial and photocatalytic functional properties of Cu-Zn modified TiO_2 nano-heterostructures, J. Photochem. Photobiol. A, 330 (2016) 44–54.
[20] K.M. Kotesh, K. Bhavani, G. Naresh, B. Srinivas, A. Venugopal, Plasmonic resonance nature of Ag-Cu/TiO_2 photocatalyst under solar and artificial light: synthesis, characterization and evaluation of H_2O splitting activity, Appl. Catal. B, 199 (2016) 282–291.
[21] A. Sasani, A. Baktash, K. Mirabbaszadeh, B. Khoshnevisan, Structural and electronic properties of Mg and Mg-Nb co-doped TiO_2 (101) anatase surface, Appl. Surf. Sci., 384 (2016) 298–303.
[22] W. Zhang, C. Li, Z. Ma, L. Yang, H. He, Effects of calcination temperature on properties of 0.5%Al-3%In-TiO_2 photocatalyst prepared using sol-gel method, J. Adv. Oxid. Technol., 19 (2016) 119–124.
[23] S.K. Kansal, S. Sood, A. Umar, Photocatalytic degradation of Eriochrome Black T dye using well-crystalline anatase TiO_2 nanoparticles, J. Alloys Compd., 581 (2013) 392–397.
[24] J.L. Ropero-Vega, A. Aldana-perez, R. Gomez, Sulfated titania [TiO_2/SO_4^{2-}]: a very active solid acid catalyst for the esterification of free fatty acids with ethanol, Appl. Catal. A, 379 (2010) 24–29.
[25] S. Javaid, M.A. Farrukh, I. Muneer, Influence of optical band gap and particle size on the catalytic properties of Sm/SnO_2–TiO_2 nanoparticles, Superlattices Microstruct., 82 (2015) 234–247.
[26] W. Zhang, T. Hu, B. Yang, P. Sun, H. He, The effect of boron content on properties of B-TiO_2 photocatalyst prepared by sol-gel method, J. Adv. Oxid. Technol., 16 (2013) 261–267.
[27] J. Tauc, R. Grigorovici, A. Vancu, Optical properties and electronic structure of amorphous germanium, Phys. Status Solidi B, 15 (1966) 627–637.